Available online at www.sciencedirect.com
SCIENCE DIRECT®
Journal of Solid State Chemistry 178 (2005) 3453–3460
JOURNAL OF SOLID STATE CHEMISTRY
www.elsevier.com/locate/jssc

Synthesis, structure, and magnetic properties of $SrMn_{1-x}Ga_xO_{3-\delta}$ ($x = 0$–0.5) perovskites

B. Dabrowski[a,b], E.N. Caspi[c,*], S. Kolesnik[a], O. Chmaissem[a,b], J. Mais[a], J.D. Jorgensen[b]

[a]*Department of Physics, Northern Illinois University, DeKalb, IL 60115, USA*
[b]*Materials Science Division, Argonne National Laboratory, Argonne, IL 60439, USA*
[c]*Physics Department, Nuclear Research Centre-Negev, P O Box 9001, 84190 Beer-Sheva, Israel*

Received 31 May 2005; received in revised form 16 August 2005; accepted 28 August 2005
Available online 4 October 2005

Abstract

We report the synthesis of $SrMn_{1-x}Ga_xO_{3-\delta}$ perovskite compounds and describe the dependence of their phase stability and structural and physical properties over extended cation and oxygen composition ranges. Using special synthesis techniques derived from thermogravimetric measurements, we have extended the solubility limit of random substitution of Ga^{3+} for Mn in the cubic perovskite phase to $x = 0.5$. In the cubic perovskite phase the maximum oxygen content is close to $3-x/2$, which corresponds to 100% Mn^{4+}. Maximally oxygenated solid solution compounds are found to order antiferromagnetically for $x = 0-0.4$, with the transition temperature linearly decreasing as Ga content increases. Increasing the Ga content introduces frustration into the magnetic system and a spin-glass state is observed for $SrMn_{0.5}Ga_{0.5}O_{2.67(3)}$ below 12 K. These properties are markedly different from the long-range antiferromagnetic order below 180 K observed for the layer-ordered compound $Sr_2MnGaO_{5.50}$ with nominally identical chemical composition.

Keywords: Perovskites; Synthesis; Neutron powder diffraction; Crystal structure; Magnetic structure

1. Introduction

The effects of local atomic order on the properties of perovskite manganites have been recently investigated with increasing interest because of remarkable changes of electronic and magnetic properties resulting from alteration of local exchange interactions [1]. To date these effects have been studied in detail only for the mixed-valent layered-ordered $RBaMn_2O_{6-2\delta}$ ($\delta = 0$ and 0.5) and randomly substituted $R_{0.5}Ba_{0.5}MnO_3$ compounds with nominally identical chemical compositions [2–8]. A large (~80 K) decrease of the ferromagnetic transition temperature, T_C, has been observed for the randomly substituted phase with $R = La$ and has been attributed to local A-site charge disordering that profoundly disturbs the coherent electronic states of the Mn–O bonds [3,8]. Randomness effects in $Pr_{0.5}Ba_{0.5}MnO_3$ with various degrees of A-site disorder have been reported in detail [5,6].

Studies of other ordered and disordered manganites are restricted by the difficulty of forming the desired atomic arrangements while preserving the overall chemical composition. The difficulty to form such phases arises in part from the limited substitution levels on the A- and B(Mn)-sites, beyond which formation of the perovskite ABO_3 phase is usually not possible because of the unfavorable tolerance factor $t = (A\text{–O})/\sqrt{2}(B\text{–O})$ of the desired composition. Here (A–O) and (B–O) are the average bond lengths of the A and B cations to oxygen. For this reason, various schemes have been developed for extending the composition range over which the perovskite phase can be formed. For example, using high-temperature synthesis at reduced oxygen pressure followed by low-temperature oxygen annealing we have recently been able to extend the solubility limits from $y = 0.4$ to 1 for $Ca_{1-y}Sr_yMnO_3$ [9] from $y = 0.6$ to 1 for $La_{1-y}Sr_yMnO_3$ and

*Corresponding author. Fax: +972 8 656 7878.
E-mail address: caspie@nrcn.org.il (E.N. Caspi).

0022-4596/$ - see front matter © 2005 Elsevier Inc. All rights reserved.
doi:10.1016/j.jssc.2005.08.031

$Pr_{1-y}Sr_yMnO_3$ [10], and obtain the complete solubility ranges for $SrFe_{1-y}Mn_yO_3$ [11] and $SrRu_{1-y}Mn_yO_3$ [12].

The parent compound $SrMnO_{3-\delta}$ of our investigation displays two different crystal structures. When synthesized in oxygen or air, $SrMnO_3$ forms in a hexagonal four-layered structure in which face-shared $MnO_{6/2}$ octahedra are present in addition to the cornered-shared ones that are characteristic for perovskites. The hexagonal phase transforms to the perovskite phase upon heating in air above 1440 °C where the oxygen content is reduced below 2.72 atoms per formula unit, as described by Negas and Roth [13]. This low oxygen content stabilizes the perovskite phase because of the reduced formal valence and resulting larger ionic size of the Mn cation, i.e., as a result of the decreased tolerance factor [14]. Thus, a method that stabilizes the perovskite phase [15,16] is the reduction of hexagonal $SrMnO_{3-\delta}$ in Ar at 1450 °C, followed by cooling to low temperatures without allowing the increase of the oxygen content, resulting in an oxygen-vacancy ordered $SrMnO_{2.5}$ compound with all Mn^{3+}. The oxygen deficient perovskites can then be fully oxygenated ($\delta = 0$) in air at low temperatures (e.g., 200–700 °C) where cation diffusion is kinetically hindered, to form a kinetically stable perovskite $SrMnO_3$ [9,17,18]. The stability of pure and Ca-substituted $SrMnO_{3-\delta}$ perovskites at temperatures higher than ~800 °C is described by the condition $t(x, T, \delta) \leqslant 1$, where t is the composition-temperature-and oxygen content-dependent tolerance factor [17,18]. For a given composition x, $t(x, T, \delta)$ is an increasing function of temperature and decreasing function of oxygen vacancy content; thus, it is possible to tune the synthesis conditions of temperature and oxygen pressure to produce the desired perovskite or hexagonal phases.

In our recent publication [19] we have reported a two-step synthesis, involving high-temperature firing in flowing Ar (~20 ppm O_2) followed by low-temperature oxygen annealing, of the randomly Ga-substituted $SrMn_{1-x}Ga_xO_{3-\delta}$ compositions with a simple cubic perovskite phase (space-group $Pm\bar{3}m$) over the composition range of $0 \leqslant x \leqslant 0.3$. The same two-step synthesis produced a layered-ordered $Sr_2MnGaO_{6-2\delta}$ (brownmillerite structure for $\delta = 0.5$ and orthorhombic (*Cmcm*) structure for $\delta = 0.25$) for $x = 0.5$. Randomly Ga-substituted compounds could not be synthesized in the perovskite structure beyond $x \approx 0.33$ using such a two-step synthesis technique because the high-temperature firing in Ar resulted in compounds with a large vacancy content $\delta \approx 0.5$, i.e., with all Mn^{3+}, which favors ordering of the Mn and Ga.

This paper describes the synthesis and properties of $SrMn_{1-x}Ga_xO_{3-\delta}$ ($x = 0-0.5$) stabilized in the perovskite phase by the random substitution of Ga for Mn. The special synthesis conditions for synthesis of randomly Ga-substituted perovskite compounds beyond $x \approx 0.33$ have been derived from thermogravimetric measurements. Structural and magnetic properties are studied for the samples with maximum oxygen content of $\delta \approx x/2$, where nearly all of the Mn is in the 4+ valence state achieved after annealing in air at 400 °C. At low temperatures these simple perovskite phases are antiferromagnets for $x = 0-0.4$. The transition temperature decreases linearly with the increase of the diamagnetic Ga^{3+} content. The $x = 0.5$ composition $SrMn_{0.5}Ga_{0.5}O_{2.67(3)}$ shows a spin-glass state. Magnetic properties of these randomly substituted compositions are compared with layered-ordered antiferromagnetic $Sr_2MnGaO_{5.5}$ compound [19] with nominally identical chemical composition and similar Mn^{4+} valence state.

2. Experimental procedures

2.1. Synthesis

The objective of this work was to synthesize and characterize samples of randomly substituted polycrystalline $SrMn_{1-x}Ga_xO_{3-\delta}$ with the perovskite structure over the range of Ga concentrations that would include $x = 0.5$. Samples were synthesized from stoichiometric mixtures of $SrCO_3$, Ga_2O_3, and MnO_2. Pressed powder samples of $x = 0.4$ and 0.5 were initially processed using a solid state reaction method in which they were fired in air several times at various temperatures up to 1300 °C for 20 h followed by either slow cooling or quenching. This synthesis procedure did not yield single-phase perovskite samples for any composition. Extensive powder X-ray diffraction (at room temperature using a Rigaku D/MAX diffractometer) was used to examine the products after each synthesis step.

Application of synthesis method used for $SrMnO_{3-\delta}$ of forming single-phase oxygen-deficient perovskites in flowing Ar gas at 1300–1335 °C (~20 ppm O_2) has been successful only for the $x = 0.1$, 0.2, and 0.3 compositions [19]. Based on thermogravimetric data (that will be discussed in following sections) single-phase oxygen-deficient perovskites with $x = 0.4$ and 0.5 have been obtained at 1220–1235 °C by firing for 20 h in flowing 1% O_2/Ar gas mixture followed by fast cooling to room temperature in a quartz tube by removing it from the hot furnace. Oxygen deficient single-phase samples with layered-ordered and randomly substituted structures were obtained from Ar at 1300 °C and fast cooling from 1% O_2/Ar gas mixture at 1235 °C, respectively. Oxygen contents were determined by measuring the mass increase resulting from annealing in air at 400 °C. Thermogravimetric and neutron powder diffraction were used to verify the oxygen content.

In a second synthesis step, oxygen was added to $x = 0.4$ and 0.5 samples by annealing in air at temperatures low enough that cation diffusion could not occur. This resulted in final oxygen contents of approximately $3.00-x/2 \pm 0.01$ ($\delta = x/2$) atoms per formula unit. These oxygen contents are the maximally oxygenated compositions with formal valences of Ga and Mn of 3+ and 4+, respectively.

2.2. Thermogravimetric (TGA) measurements

Thermogravimetric analysis (TGA) measurements were used to study the behavior of these materials as a function of temperature and oxygen partial pressure in order to determine the special synthesis conditions. All TGA measurements were performed on a Cahn TG171 thermobalance. For increased accuracy, samples as large as 1 g (consisting of small chunks) were heated in alumina crucibles suspended on Pt wires. The weights of the samples were measured to a precision of 2 μg. Empty-crucible TGA runs were used for calibration and buoyancy corrections. Reproducibility of the data was checked several times using identical TGA conditions for samples with the same x values.

Absolute oxygen contents were determined by assuming that the oxygen content of the single-phase samples after final oxygenation at low temperatures is $3-x/2$. Rietveld refinement of the oxygen site occupancy using neutron powder diffraction data from maximally oxygenated samples (to be described later) is consistent with this designation within two standard deviations. The oxygen contents determined in this way were self-consistent showing a change of $\sim (1-x)/2$ among samples annealed in Ar at 1300 °C (Mn^{3+}) and after final oxygenation at low temperatures (Mn^{4+}) for $x = 0.3-0.5$. They were also consistent with results from hydrogen reduction on the Ga-free parent compound, $SrMnO_{3-\delta}$ [17,18].

2.3. Energy dispersive X-ray spectroscopy measurements

Sample morphology and relative compositions were studied by electron microscopy using a Hitachi S-4700-II scanning electron microscope for fully oxygenated $SrMn_{1-x}Ga_xO_{3-0.5x}$ compounds. Scanning electron micrographs are shown in Fig. 1(a) and (b) for $SrMnO_3$ and nominal $SrMn_{0.5}Ga_{0.5}O_{2.75}$, respectively. These polycrystalline materials form grains of over 10 μm in size. Large-size grains, absence of voids, and smooth and sharp grain boundary indicate that the fast synthesis of the perovskite phase is achieved by presence of a liquid phase.

Energy dispersive X-ray spectroscopy (EDXS) analysis was performed by collecting 15–30 EDXS spectra for each composition at various locations across the surface of a sintered pellet. The effective Mn and Ga contents for $SrMn_{1-x}GaxO_{3-0.5x}$ as determined from the EDXS data are shown in Fig. 1(c). The effective content was calculated by dividing the percentage of each element by the percentage of strontium determined from the same EDXS spectra. Straight lines are the expected dependencies of the Mn and Ga contents with respect to the nominal Ga content x. The effective Ga content x_{eff}(Ga) is in a good agreement with the expected value x. The effective Mn content x_{eff}(Mn) is systematically lower than the expected value $x_{eff}(Mn) = 1-x$. Since no impurity phase is observed neither in the XRD data nor in the NPD data (see below and Fig. 5), we suggest that the missing fraction of manganese is caused by systematic error in the EDXS analysis. However, in view of neutron powder diffraction measurements discussed in following sections, the presence of a small concentration of vacancies on the Mn(Ga) sites can not be ruled out.

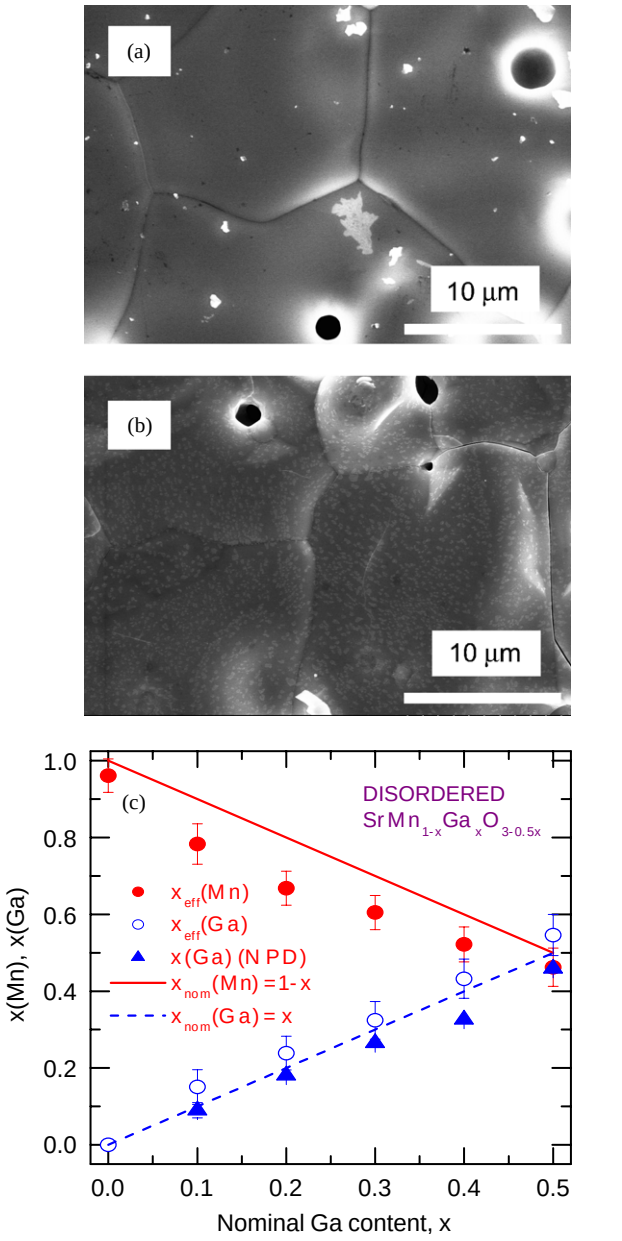

Fig. 1. Scanning electron micrographs of (a) $SrMnO_3$ and (b) $SrMn_{0.5}Ga_{0.5}O_{2.75}$. (c) Effective contents of Mn (●) and Ga (○) in nominal $SrMn_{1-x}Ga_xO_{3-\delta}$ determined from EDXS experiments alongside with refined content of Ga (▲) determined from NPD data as a function of nominal Ga concentration. Lines are the nominal values of Mn and Ga concentrations.

2.4. Neutron powder diffraction (NPD) measurements

Time of flight neutron powder diffraction data were collected on the Special Environment Powder Diffract-

ometer (SEPD) [20] at Argonne's Intense Pulsed Neutron Source (IPNS). Diffraction data were collected for the maximally oxygenated samples $SrMn_{1-x}Ga_xO_{3-\delta}$ with $x = 0.4$ and 0.5 at RT (~295 K). High-resolution backscattering data ($2\theta = 144.85^\circ$, Bank 1) were analyzed using the Rietveld method with the GSAS (EXPGUI) suite [21,22].

2.5. Susceptibility and magnetization measurements

Alternating current (ac) susceptibility and static magnetization were measured using a Physical Property Measurement System 6000 (Quantum Design) in the temperature range 5–400 K. "Zero-field-cooled" (ZFC) magnetization was measured after cooling in a zero magnetic field and switching on a magnetic field of 1 kOe at a low temperature. "Field-cooled" (FC) magnetization was measured on cooling in the magnetic field. Thermoremanent magnetization was measured after cooling in the magnetic field and switching the magnetic field to zero. ZFC, FC and thermoremanent magnetization measurements were taken in the temperature range of 5–50 K.

3. Results and discussion

Throughout this paper the nominal Mn and Ga compositions as well as the oxygen content refined from the NPD will be used to define various samples. Mn and Ga values determined by EDXS and NPD measurements are shown in Fig. 1(c). TGA and NPD refined oxygen contents are given in Table 1.

3.1. TGA and X-ray diffraction (XRD) investigation of the synthesis process

The TGA measurements, combined with XRD studies of samples obtained from several temperatures and atmospheres, show why a special two-step synthesis process is needed to make single-phase samples with randomly substituted Mn and Ga for $x = 0.4$ and 0.5. Fig. 2 shows the oxygen contents upon heating in Ar (1.2 °C/min) of the single-phase, randomly substituted and maximally oxygenated $x = 0-0.5$ samples. The randomly substituted perovskites begin to lose oxygen near 350 °C and, then, in the temperature range of 830–1130 °C, display plateaus in the oxygen contents. XRD studies of samples quenched from various temperatures show that the perovskite phase is maintained before these plateaus are reached (denoted by an arrow), at which point the materials partially decompose into mixtures of phases that include a hexagonal 4-layered structure as a major impurity phase [13]. Further heating introduces more oxygen vacancies and single-phase randomly substituted perovskite phase is achieved for $x = 0.0-0.3$ and layered-ordered phase is achieved for $x = 0.5$ after 14 h holding in Ar at 1300 °C (at 1400 °C for $x = 0$) [19]. These structural phases are maintained upon cooling to room temperature in Ar so that no oxygen uptake is allowed. The $x = 0.4$ sample obtained this way is mixed-phase with the randomly substituted perovskite and the layered-ordered phase as majority phases. The final oxygen-vacancy contents of these samples are 2.56, 2.58, 2.55, 2.52, 2.49, and 2.49 for $x = 0$, 0.1, 0.2, 0.3, 0.4, and 0.5, respectively. The decomposition of the perovskite phase around 800–1000 °C (depending on Ga content), followed by formation of a single phase at higher temperatures has been discussed in detail in terms of diffusion kinetics and tolerance factor arguments [17,18].

Table 1
Room temperature structural parameters of maximally oxygenated $SrMn_{1-x}Ga_xO_{3-\delta}$ samples as a function of nominal Ga content (x)

X		0.4	0.5
A (Å)		3.84443 (2)	3.85761 (2)
V (Å^3)		56.819 (1)	57.406 (1)
Sr	B (Å^2)	0.85 (6)	1.22 (7)
(Mn,Ga)	Ga SOF	0.326 (2)	0.459 (6)
	B (Å^2)	−1.3 (1)	5.0 (4)
O	SOF	0.94 (1)	0.89 (1)
	U_{11} (Å^2)	0.79 (8)	0.61 (4)
	$U_{22}(=U_{33})$ (Å^2)	1.36 (4)	1.30 (3)
(Mn,Ga)–O (Å)		1.92221 (1)	1.92881 (1)
T_t (K)		62 (4)	12 (2)
TGA Oxygen		2.80	2.75
R_{wp} (%)		6.57	5.03
R_{exp} (%)		5.19	3.85

Rietveld analyses of neutron diffraction data were performed using the cubic space-group $Pm\bar{3}m$ with the following atom positions: Sr at $1b(\frac{1}{2},\frac{1}{2},\frac{1}{2})$, (Mn,Ga) at $1a(0,0,0)$, and O at $3d(\frac{1}{2},0,0)$. SOF is site occupation factor. B (U_{ij}) is the isotropic (anisotropic) thermal displacement parameter. TGA oxygen is the oxygen content derived by TGA. It should be compared to 3*SOF. Numbers in parentheses are the standard deviations of the last significant digit. The fitted weighted profile (R_{wp}), and expected (R_{exp}) agreement factors are also given. For $x = 0.4$ $T_t \equiv T_N$, the antiferromagnetic transition temperature. For $x = 0.5$ $T_t \equiv T_f$ the spin-glass freezing temperature. T_t is measured by ac-susceptibility.

TGA studies in 1% O_2 in Ar of the air annealed samples obtained from TGA experiments in Ar show how the single-phase randomly substituted $x = 0.4$ and 0.5 compounds can be obtained. Fig. 3 shows the oxygen contents of the single-phase randomly substituted $SrMn_{0.7}Ga_{0.3}O_{2.83(2)}$, multi-phase nominal $SrMn_{0.6}Ga_{0.4}O_{2.8}$, and single-phase layered-ordered $Sr_2MnGaO_{5.52(1)}$ samples upon heating (1.0 deg/min) in 1% O_2 in Ar [19]. Oxygen loss begins near 300 °C (denoted by A) and proceeds to ~970, 860, and 880 °C (denoted by B and B′) for $x = 0.3$, 0.4, and 0.5, respectively. The oxygen contents then increase in the temperature ranges of 970–1100, 860–1100, and 880–1160 °C for $x = 0.3$, 0.4, and 0.5, respectively. XRD studies show that in analogy to TGA experiments in Ar, the perovskite phases decompose at temperature range 970–1100 °C while the layered-ordered phase decomposes at lower temperature range 860–1100 °C (denoted by B′). Further heating introduces more oxygen vacancies (denoted by C) and the randomly substituted

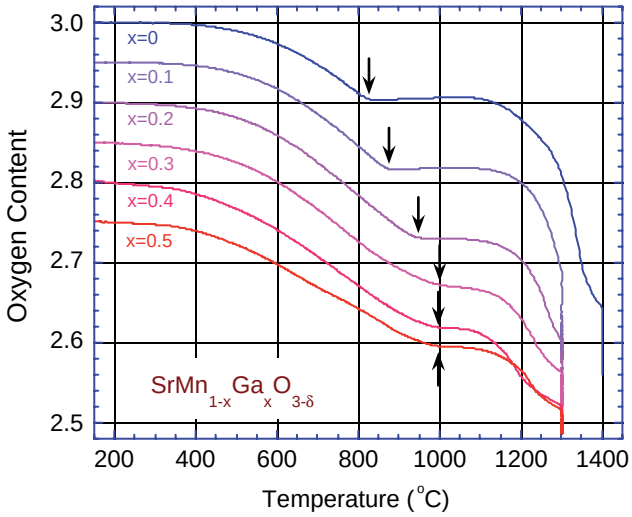

Fig. 2. Thermogravimetric measurements in Ar (1.2 deg/min) of the single-phase maximally oxygenated $SrMn_{1-x}Ga_xO_{3-0.5x}$ perovskites. Arrows indicate temperatures of decomposition of the perovskite phase to mixtures of phases that include a hexagonal 4-layered structure.

perovskite phase begins to form at 1200, 1210, and 1220 °C when oxygen content is below 2.75, 2.73, and 2.64 (denoted by D) for $x = 0.3$, 0.4, and 0.5, respectively. A single-phase is achieved after 1 h holding at 1300 °C (denoted by E) for all samples. These samples increase their oxygen contents but remain single-phase (denoted by F) upon cooling (1.0 deg/min) in 1% O_2 in Ar to ~1220, 1170, and 1150 °C for $x = 0.3$, 0.4, and 0.5, respectively. Further cooling introduces more oxygen and the perovskite phases partially decompose when oxygen content is above 2.61, 2.59, and 2.57 for $x = 0.3$, 0.4, and 0.5, respectively.

Fig. 4 summarizes characteristic oxygen contents that define stability ranges of the single-phase and multi-phase perovskites for $x = 0-0.5$ at the synthesis temperature of ~1200–1300 °C. The $SrMn_{1-x}Ga_xO_{3-\delta}$ perovskites decompose when oxygen content is below 2.5 (i.e., for $\delta > 0.5$) for all x. In addition, because the maximum possible oxygen content after annealing in air is $3-x/2$, the maximum range of oxygen vacancies which can be achieved for $SrMn_{1-x}Ga_xO_{3-\delta}$ perovskites is given by $x/2 \leqslant \delta \leqslant 0.5$. All these oxygen compositions can be attained by annealing single-phase samples under appropriate atmosphere (e.g., air, argon, or hydrogen) at low enough temperatures.

With increasing Ga substitution, decreased oxygen content (increased δ) is required to stabilize the randomly substituted perovskite phase. At low oxygen contents of less than ~2.55 ($\delta > 0.45$) the ordered phases are observed for $x \approx 0$ (oxygen vacancy ordered) and for $x \approx 0.5$ (the oxygen vacancy and the *B*-site cation layered-ordered phase). As a result, the range of oxygen content where the randomly substituted perovskites can be synthesized narrows with increasing x. It becomes very small 2.53–2.59 ($0.47 > \delta > 0.41$) and 2.54–2.57 ($0.46 > \delta > 0.43$) for $x = 0.4$ and 0.5, respectively. When oxygen content is below this range the multiphase sample forms for $x = 0.4$ and the single-phase layered-ordered phase forms for $x = 0.5$. When oxygen content is above this range the randomly substituted perovskites decompose into mixtures of phases that include a hexagonal four-layered structure.

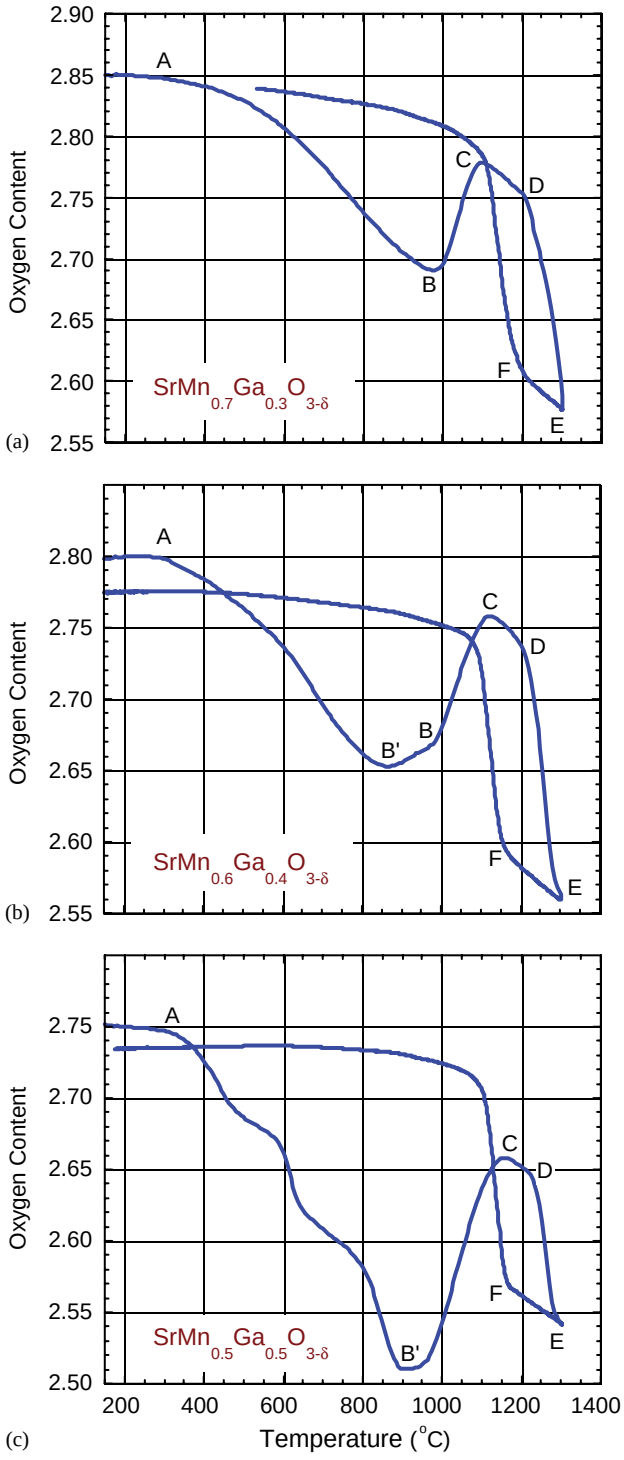

Fig. 3. Thermogravimetric measurements in 1% O_2 in Ar of the air annealed samples obtained from TGA experiments in Ar for single-phase randomly substituted $SrMn_{0.7}Ga_{0.3}O_{2.83(2)}$ (a), multi-phase nominal $SrMn_{0.6}Ga_{0.4}O_{2.8}$ (b), and single-phase layered-ordered $Sr_2MnGaO_{5.52(1)}$ (c). Various reduction and oxidation steps are denoted by A–E (see text).

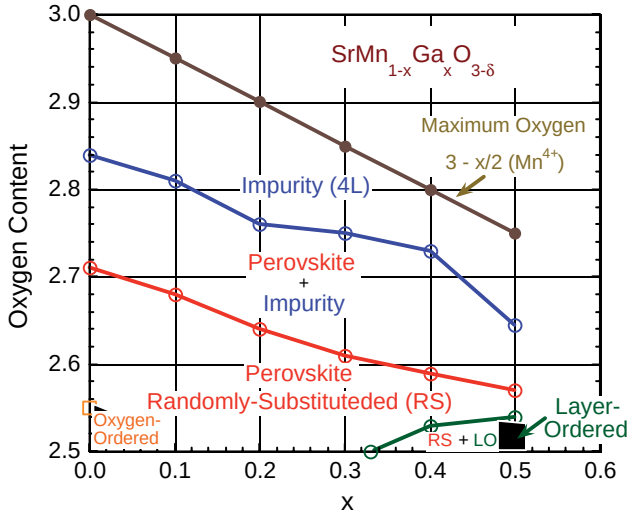

Fig. 4. Summary of characteristic oxygen contents that define stability ranges of the single-phase and multi-phase $SrMn_{1-x}Ga_xO_{3-\delta}$ perovskites with randomly substituted (RS) and layer-ordered (LO) *B*-site cations Mn and Ga for $x = 0-0.5$ at the synthesis temperature of ~1200–1300 °C.

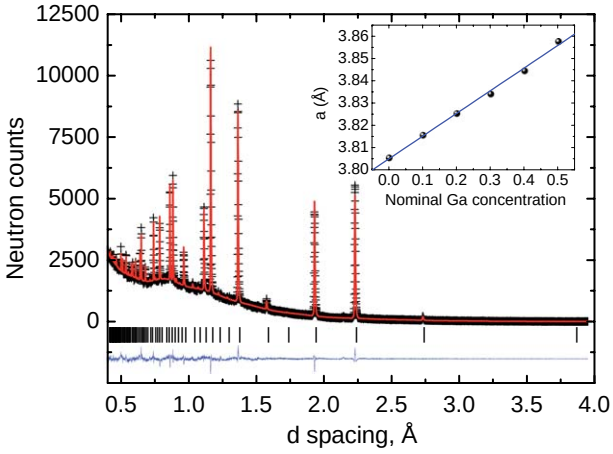

Fig. 5. Best-fit Rietveld refinement using time-of-flight neutron powder diffraction data at RT for nominal $SrMn_{0.5}Ga_{0.5}O_{2.67(3)}$. Plus symbols are observed data, and continues lines are the calculated profile and the difference. For structural details see Table 1. Inset: lattice parameter *a* (Å) as a function of nominal Ga concentration, *x*, in $SrMn_{1-x}Ga_xO_{3-\delta}$ obtained by Rietveld refinement using RT (~295 K) neutron diffraction data (Table 1; [9,19]). The solid line is a best fit of the data. Error bars are smaller than the symbol size.

The range of oxygen contents where the randomly substituted perovskite coexists with impurity phases was determined from points D (upper bound) and F (lower bound) of Fig. 3. The fact that the oxygen content range is so small and the oxygen content has to be preserved on cooling to prevent decomposition explains why the randomly substituted perovskites have not been obtained previously for $x > 0.3$. TGA and X-ray diffraction measurements show that to obtain single-phase randomly substituted perovskites the synthesis at high temperature has to be done under controlled oxygen pressure as described earlier.

The synthesis of perovskite $SrMn_{1-x}Ga_xO_{3-\delta}$ with randomly substituted Mn and Ga over an extended compositional range is important for several reasons. It demonstrates the usefulness of the thermogravimetric analysis in determining unique synthesis routes for achieving desired compositions. The synthesis of $SrMn_{1-x}Ga_xO_{3-\delta}$ allows the investigation of a composition-structure-properties phase diagram over the complete range of substitutions $0 \leqslant x \leqslant 0.5$. It provides a unique opportunity for the comparison of magnetic and resistive properties of the randomly mixed $SrMn_{0.5}Ga_{0.5}O_{2.75}$ and layer-ordered $Sr_2MnGaO_{5.50}$ compounds with nominally identical chemical compositions. Moreover, achieving the synthesis of $SrMn_{1-x}Ga_xO_{3-\delta}$ compounds over this extended composition range allows the future study of their mixed electron and oxygen ion conducting properties and comparison with similar fast ion conducting compounds of $LaGaO_3$ [23] and $La_{1-y}Sr_yFe_{1-x}Ga_xO_{3-\delta}$ [24].

3.2. Structural and magnetic properties

The RT NPD data for maximally oxygenated samples with $x = 0.1$, 0.2, and 0.3 were presented in our previous work [19] confirming that the samples are single-phase with the cubic pervoskite structure (space-group $Pm\bar{3}m$) with Mn, and Ga randomly distributed on the *B* cation site. The RT NPD data show similar behavior for maximally oxygenated samples with $x = 0.4$ and 0.5. Reflections in NPD patterns of both samples were indexed in the cubic perovskite structure, space-group $Pm\bar{3}m$, and the structures were refined accordingly using the Rietveld method (cf. Fig. 5). Refined structural parameters are summarized in Table 1.

Refined cell parameters as a function of nominal Ga concentration, *x*, are depicted in Fig. 5 (inset) along with the published cell parameter of cubic $SrMnO_3$ [9]. The linear dependence of the cubic cell parameter on *x* confirms the existence of a solid solution of Ga in the $SrMnO_3$ perovskite structure over the wide composition range of $0 \leqslant x \leqslant 0.5$, a significant extension of the solid solution range previously reported by us (cf. Fig. 5 in Ref. [19]).

The refined Ga occupancies deduced from the Rietveld analysis of the NPD data, are consistently smaller than the effective Ga concentration values measured using the EDXS measurement (Fig. 1). The difference is nearly constant within one standard deviation leading to the supposition that a systematical error is present for one or both of the two methods. In the EDXS method the effective Mn and Ga concentrations were determined separately without forcing full occupancy of the *B* site cation. In Rietveld analysis, only one variable can be refined for the *B* site occupancy. We assumed full occupancy of the site and refined the Ga concentration.

Similar differences in *B*-cation concentration values determined by the EDXS and NPD methods were reported previously for $SrRu_{1-v}O_3$ [25], where it was suggested that

there is a systematic error in modeling the crystal structure by Rietveld method. One source of difficulty in modeling the perovskite structure with randomly occupied *B*-site by the Mn and Ga ions could be due to a large fraction of oxygen atoms significantly shifted away from the normal octahedral sites dictated by the pervoskite matrix. In present refinements the oxygen atoms positioned in the distinctive tetrahedral coordination of Ga^{3+} would not be modeled correctly for the perovskite structure. Significant local displacements of the oxygen atoms from normal positions and corresponding displacements of the Ga ions could be the origin of a lower than expected oxygen and Ga/Mn occupancies listed in Table 1. In addition, it is possible that a small fraction of vacancies formed on the *B*-cation site for some of the $SrMn_{1-x}Ga_xO_{3-\delta}$ samples.

The ac susceptibilities, χ, vs. temperature are presented in Fig. 6(a) for the $x = 0.4$, and 0.5 samples. For $x = 0.4$, paramagnetic behavior is observed for temperatures above ~75 K. A small inflection in the $\chi(T)$ curve at ~65 K signals an antiferromagnetic transition to a magnetically ordered phase as identified by its similarity to anomalies observed

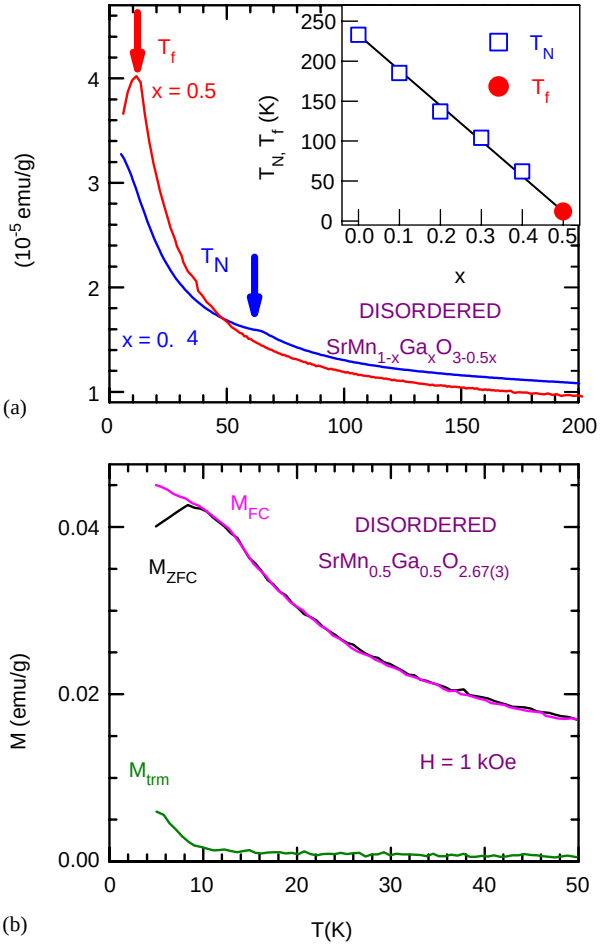

Fig. 6. (a) Temperature dependencies of the magnetic susceptibility of $SrMn_{0.6}Ga_{0.4}O_{2.82(3)}$ and $SrMn_{0.5}Ga_{0.5}O_{2.67(3)}$. The Neel temperatures T_N and the spin freezing temperature T_f are marked as arrows. (b) "zero-field-cooled" (ZFC), "field-cooled" (FC), and thermoremanent (trm) magnetizations for $SrMn_{0.5}Ga_{0.5}O_{2.67(3)}$.

in the $\chi(T)$ curves for the $x = 0-0.3$ samples (Fig. 6 in Ref. [19]). The transition temperature for $SrMn_{0.6}Ga_{0.4}O_{2.82(3)}$ was defined in analogy to the $x = 0-0.3$ samples as the temperature for which the slope of the derivative $d\chi/dT$ is maximum. The value of $T_N = 62(4)$ K was found to agree very well with previously determined linear dependence of T_N's on composition for other maximally oxygenated $SrMn_{1-x}Ga_xO_{3-0.5x}$ materials [see: inset to Fig. 6(a)]. The increase of susceptibility at lower temperatures is most likely caused by small amounts of magnetic impurities.

The ac susceptibility for the disordered $SrMn_{0.5}Ga_{0.5}O_{2.67(3)}$ sample shows a cusp at $T_f = 12$ K [Fig. 6(a)], characteristic of a transition into a spin-glass state. A similar cusp was observed previously for the oxygen deficient $SrMn_{0.7}Ga_{0.3}O_{2.50(2)}$ sample (Fig. 6 in Ref. [19]). DC magnetization measurements show a divergence of the ZFC and FC measurements below T_f [Fig. 6(b)], again in agreement with a typical low-temperature spin glass state behavior. These findings, as well as the presence of the thermoremanent magnetization [Fig. 6(b)] below T_f confirm that the maximally oxygenated $x = 0.5$ sample displays a spin-glass magnetic ground sate.

The observed magnetic behavior of the maximally oxygenated perovskite compounds $SrMn_{1-x}Ga_xO_{3-x/2}$, previously reported by us for the $x = 0.1-0.3$ compositions [19], can now be extended to higher Ga doping levels $x = 0.5$. As we suggested previously [19], the effects of dilution resulting from the Ga substitution and the associated changes in the oxygen sublattice set by the $Mn^{3/4+}$ valence govern the evolution of the magnetic interactions in the $SrMn_xGa_{1-x}O_{3-\delta}$ system. The Good-enough-Kanamori rules of superexchange predict strictly antiferromagnetic interactions among Mn^{4+} ions in $SrMn^{4+}O_3$. Replacing Mn with Ga in $SrMnO_3$ results in weaker antiferromagnetic interactions caused by both the dilution of the matrix of magnetic ions with randomly distributed diamagnetic Ga^{3+} ions, and the gradual introduction of random oxygen vacancies. For a constant Ga^{3+} content, increased oxygen vacancy content further suppresses antiferromagnetic interactions through disorder and introduction of the mixed ferro- and anti-ferromagnetic interactions among the Mn^{3+} and Mn^{4+} ions.

Combining our present results for the perovskites with previous work [19] on layered-ordered $x = 0.5$ compound allows further study the effect of *B*-cation disorder on the magnetic properties. The maximally oxygenated *B*-cation disordered $x = 0.5$ sample exhibits spin-glass behavior with freezing temperature as low as 12 K, whereas the *B*-cation ordered $x = 0.5$ sample shows long-range antifferomagnet order below $T_N \approx 180$ K [19,26]. Both samples have similar concentrations of diamagnetic Ga^{3+} ions, as well as similar amounts of disordered oxygen vacancies. In both samples, local antiferromagnetic interactions are expected to take place between Mn^{4+} ions through the superexchange mechanism. In addition, in both samples, similar amounts of magnetic frustration among Mn^{4+} ions are introduced by missing magnetic links due to random oxygen vacancies,

yet, while the layered ordered $Sr_2MnGaO_{5.5}$ sample orders antiferromagnetically, the additional frustration introduced by the Mn/Ga disorder in perovskite $SrMn_{0.5}Ga_{0.5}O_{2.67(3)}$ is sufficient to prevent any long-range ordering, thus resulting in the spin-glass state. Similar effects of disorder on the magnetic properties of perovskite related materials was observed for the (La,Ba)MnO_3 system [3]. There, the layer ordered $LaBaMn_2O_6$ compound orders ferromagnetically at $T_C \approx 320$ K, while the disordered $La_{0.5}Ba_{0.5}MnO_3$ compound with identical overall chemical composition orders ferromagnetically below $T_C \approx 240$ K, a 25% reduction in T_C [3]. It is thus demonstrated here that various forms of disorder, either on the *A*- or *B*-cation sublattices, or the oxygen vacancies, contribute to the weakening of long-range magnetic interactions. The combined effect of the *B*-cation disorder and the random distribution of oxygen vacancies in $SrMn_{0.5}Ga_{0.5}O_{2.67(3)}$ studied here leads to complete vanishing of the long range order at this composition.

4. Conclusions

Using information gained from the thermogravimatric measurements we have succeeded in extending the solid solution to $x = 0.5$ for $SrMn_{1-x}Ga_xO_{3-\delta}$ perovskites. Using NPD, XRD, EDXS, ac-, and dc-susceptibility measurements, we have studied the structural and magnetic properties of the maximally oxygenated samples. All studied samples crystallize in the cubic $Pm\bar{3}m$ structure with *B*-site (Mn/Ga) and oxygen vacancy disorder. The lattice parameter *a* linearly increases with *x*.

Compositions $0 \leqslant x \leqslant 0.4$ order antiferromagnetically with transition temperatures decreasing with increasing *x* due to increasing disorder on Mn/Ga-sites and disruptions of the Mn^{4+}–O–Mn^{4+} network caused by increasing oxygen vacancy concentrations. Eventually, for $x = 0.5$ and $\delta \approx 0.5$ the amount of magnetic frustration is large enough to induce a spin-glass state. Upon reducing the oxygen content of $x = 0.3$ samples further suppression of antiferromagnetic interactions is observed through increased disorder and introduction of mixed ferro- and anti-ferromagnetic interactions among the Mn^{3+} and Mn^{4+} ions.

The large effect of *B*-site disorder on the magnetic interactions is observed even for a similar amount of oxygen vacancies $\delta \approx 0.5$. This is seen by comparing the long range antiferromagnetic ($T_N \approx 180$ K) *B*-cation ordered $Sr_2MnGaO_{5.50(2)}$ compound with the spin-glass ($T_f \approx 12$ K) *B*-cation disordered $SrMn_{0.5}Ga_{0.5}O_{2.67(3)}$ perovskite. By developing new synthesis schemes it is possible to tune the amount of the *A*- and *B*-site order as well as the oxygen content to enhance the desired properties of perovskites.

Acknowledgments

Work at NIU was supported by the NSF-DMR-0302617 and by the US Department of Transportation. At ANL work was supported by the US Department of Energy, Division of Basic Energy Science—Materials Sciences, under contract No. W-31-109-ENG-38.

References

[1] Y. Tokura, N. Nagaosa, Science 288 (5465) (2000) 462–468.
[2] F. Millange, V. Caignaert, B. Domenges, B. Raveau, E. Suard, Chem. Mater. 10 (1998) 1974.
[3] B. Dabrowski, O. Chmaissem, J. Mais, S. Kolesnik, J.D. Jorgensen, S. Short, Mat. Res. Soc. Symp. Proc. 718 (2002) 169.
[4] T. Nakajima, H. Kageyama, H. Yoshizawa, K. Ohoyama, Y. Ueda, J. Phys. Soc. Japan 72 (2003) 3237.
[5] D. Akahoshi, M. Uchida, Y. Tomioka, T. Arima, Y. Matsui, Y. Tokura, Phys. Rev. Lett. 90 (2003) 177203.
[6] Y. Ueda, T. Nakajima, J. Phys.: Condens. Matter 16 (2004) S573.
[7] T. Nakajima, H. Yoshizawa, Y. Ueda, J. Phys. Soc. Japan 73 (2004) 2283.
[8] T.J. Sato, J.W. Lynn, B. Dabrowski, Phys. Rev. Lett. 93 (2004) 267204.
[9] O. Chmaissem, B. Dabrowski, S. Kolesnik, J. Mais, D.E. Brown, R. Kruk, P. Prior, B. Pyles, J.D. Jorgensen, Phys. Rev. B 64 (2001) 134412.
[10] O. Chmaissem, B. Dabrowski, S. Kolesnik, J. Mais, J.D. Jorgensen, S. Short, Phys. Rev. B 67 (2003) 094431.
[11] S. Kolesnik, B. Dabrowski, J. Mais, D.E. Brown, O. Chmaissem, R. Kruk, C.W. Kimball, Phys. Rev. B 67 (2003) 144402.
[12] B. Dabrowski, et al., unpublished.
[13] T. Negas, R.S. Roth, J. Solid State Chem. 1 (1970) 409.
[14] R.D. Shannon, Acta Crystallogr. A 32 (1976) 751.
[15] V. Caignaert, J Magn. Magn. Mater. 166 (1997) 117.
[16] K.R. Poeppelmeier, M.E. Leonowicz, J.C. Scanion, J.M. Longo, W.B. Yelon, J. Solid State Chem. 45 (1982) 71.
[17] B. Dabrowski, O. Chmaissem, J. Mais, S. Kolesnik, J.D. Jorgensen, S. Short, J. Solid State Chem. 170 (2003) 154.
[18] B. Dabrowski, O. Chmaissem, J. Mais, S. Kolesnik, Acta Phys. Polon. A 105 (2004) 45.
[19] E.N. Caspi, M. Avdeev, S. Short, J.D. Jorgensen, B. Dabrowski, O. Chmaissem, J. Mais, S. Kolesnik, J. Solid State Chem. 177 (2004) 1456.
[20] J.D. Jorgensen, J. Faber Jr., J.M. Carpenter, R.K. Crawford, J.R. Haumann, R.L. Hitterman, R. Kleb, G.E. Ostrowsky, F.J. Rotella, T.G. Worlton, J. Appl. Cryst. 22 (1989) 321.
[21] A.C. Larson, R.B. Von Dreele, Los Alamos Natl. Laboratory, LAUR (2004) 86–748.
[22] B.H. Toby, J. Appl. Cryst. 34 (2001) 210.
[23] M. Feng, J.B. Goodenough, Eur. J. Solid State Inorg. Chem. 31 (1994) 663.
[24] M.V. Patrakeev, E.B. Mitberg, A.A. Lakhtin, I.A. Leonidov, V.L. Kozhevnikov, V.V. Kharton, M. Avdeev, F.M.B. Marques, J Solid State Chem. 167 (2002) 203.
[25] B. Dabrowski, O. Chmaissem, P.K. Klamut, S. Kolesnik, M. Maxwell, J. Mais, Y. Ito, B.D. Armstrong, J.D. Jorgensen, S. Short, Phys. Rev. B 70 (2004) 014423.
[26] V. Yu. Pomjakushin, A.M. Balagurov, T.V. Elzhov, D.V. Sheptyakov, P. Fischer, D.I. Khomskii, V. Yu. Yushankhai, A.M. Abakumov, M.G. Rozova, E.V. Antipov, M.V. Lobanov, S. Billinge, Phys. Rev. B 66 (2002) 184412.